Polymer Degradation and Stability 95 (2010) 2430–2444

Contents lists available at ScienceDirect

Polymer Degradation and Stability

journal homepage: www.elsevier.com/locate/polydegstab

Sensitivity analysis of a predictive model for the fire behaviour of a sandwich panel

Antonio Galgano [a], Colomba Di Blasi [a,*], Eva Milella [b]

[a] Dipartimento di Ingegneria Chimica, Università degli Studi di Napoli "Federico II", P.le V. Tecchio, 80125 Napoli, Italy
[b] IMAST SCarl, P.le E. Fermi, Granatello, 80055 Portici, Italy

ARTICLE INFO

Article history:
Received 2 November 2009
Received in revised form
10 June 2010
Accepted 18 August 2010
Available online 24 August 2010

Keywords:
Glass-reinforced plastics
Sandwich panels
Mathematical modelling
Fire response
Sensitivity analysis

ABSTRACT

A sensitivity analysis to assumptions and input variables is carried out for a predictive model previously developed [1] for the fire response of a glass-fibre/polyester panel and a glass-fibre/polyester–Vermiculux sandwich. It is an unsteady, one-dimensional model using the porous medium approximation and a constant gas pressure with two-step, finite rate kinetics for the thermal decomposition and combustion of the polymeric resin, moisture evaporation described by an Arrhenius rate law, heat and mass transfer by convection, heat conduction and radiation described by effective thermal conductivities, variation of the volumetric fractions of the polymeric resin and the moisture with the conversion degree, effective specific heats, external heat transfer resistances and surface ablation. The strongest impact on the model predictions is exerted by the imposed external heat flux with variations on the characteristic process times between 49 and 774%. An important role in sample heating/conversion is also played by surface ablation and/or external heat transfer resistance with variations up to 30–72% or, when ablation is disregarded, with temperatures along the core layer well below those of the degrading skin. These are also significantly affected by surface heat losses, with the assumption of adiabatic bottom surface leading to heterogeneous ignition of the lower skin, and evaporation of moisture with variations in the characteristic times up to 35%. The model for the effective thermal conductivity of the fibre-reinforced skin (the Parallel, the Maxwell–Eucken and the Effective Medium Theory models versus the Series model) is also important resulting in characteristic time variations up to 35%. The absence of local thermal equilibrium between the condensed and the gas/vapour phase and the kinetic details of the polymer reactions are comparatively less important (maximum diminution in the characteristic times of 16%). Moreover, although over-pressures, modelled by the Darcy law, become quite high especially during the moisture evaporation stage (up to ten times the atmospheric value), their effects on the thermal response of the structure are completely negligible when structural changes are not modelled. Finally, a sensitivity analysis is also carried out to input parameters.

1. Introduction

The thermal response of composite materials exposed to fire conditions is the result of strong interactions between chemical and physical processes under highly dynamic conditions [2–9]. The application of multi-layered structures, such as sandwich panels, in spacecraft, aircraft, automotive, marine and building industries, where it is important to obtain high strength-to-weight and stiffness-to-weight ratios [10], introduce further complications, due to the different chemical and physical properties between the inner (core) and external (skin) layers and the large influences exerted by the core on the thermal response [1]. The sandwich composite used in marine applications is usually made with thin face skins of fibre-reinforced polymer laminate enchasing a thick core of ultra-light material [11]. The skins are made using a wide range of fibres and resins, including glass, carbon and Kevlar fibres and polyesters, vinyl esters and epoxies whereas the most common materials for the core layer are poly(vinyl chloride) foam, polyurethane foam and balsa. In particular, a glass-reinforced plastic (GRP) sandwich panel, consisting of GRP outer skins with calcium silicate material (Vermiculux) sandwiched between, was proposed [12] and modelled [1,12].

The mathematical modelling of the thermal response of simple or multi-layered composite structures to fire is needed to interpret the results of standard tests for material qualification and to develop multi-disciplinary design of innovative appliances, thus reducing the experimental efforts and related costs. The simplest approach,

* Corresponding author. Tel.: +39 081 7682232; fax: +39 081 2391800.
E-mail address: diblasi@unina.it (C. Di Blasi).

0141-3910/$ – see front matter © 2010 Elsevier Ltd. All rights reserved.
doi:10.1016/j.polymdegradstab.2010.08.012

producing empirical models, generally uses a pure heat conduction equation (or in any case highly simplified transport equations) and apparent chemico-physical properties which incorporate all the effects other than heat conduction. In other words the apparent specific heat takes into account the medium thermal capacity and the reaction heat whereas the apparent thermal conductivity describes all the heat transfer processes, i.e. conduction, convection and radiation. The validity of these models is, however, limited to the specific experimental conditions under which they have been developed. Instead, predictive models including a detailed description of all the processes, after experimental validation, can be confidently used over wide ranges of experimental conditions. However, the influences of the various approaches employed for the mathematical descriptions on the qualitative and quantitative trends of the predictions are often not clearly defined. Moreover, numerous parameters, generally not well known, need to be assigned to carry out the numerical simulation of the conversion process. Therefore, adequate sensitivity analyses of predictive models can be useful to better establish the level of uncertainty in the predictions and to individuate the aspects of the model that deserve further improvements or can be simplified.

As anticipated, the prediction of the fire response of sandwich panels has been given consideration only for the GRP/Vermiculux/GRP system by the empirical model [12] by Looyeh et al. and the predictive model [1] by Galgano et al. In the development of the more recent predictive model [1], special care has been put in the formulation of experimentally validated sub-models for the chemical reaction kinetics and effective thermal conductivities and specific heats of skins and core. It consists of the one-dimensional unsteady conservation equations taking into account heat transfer by convection and conduction, convective mass transfer, surface heat transfer, effective thermal conductivity, moisture evaporation, ablation of the heat-exposed surface, and polymer decomposition and combustion. Moreover, the model has been experimentally validated by means of measured temperature versus time profiles for the single skin and the sandwich panels. However, the numerical simulation has been limited only to the cases of a single glass-fibre/polyester panel and a glass-fibre/polyester–Vermiculux sandwich subjected to an assigned hydrocarbon flame.

The general scope of this study is to apply the comprehensive transport model for sandwich panels under fire conditions, already developed [1], to study the impact of some assumptions on the model predictions and to carry out a sensitivity analysis of the model outputs to input parameters, thus further contributing for the development of effective models and the improvement of knowledge about the thermal response of sandwich panels to fires. The modelling aspects that are examined here include the description of the heat transfer between the sample and the external source and between the volatile products and the solid phase, the models for the effective thermal conductivity and the description of pressure and velocity variations.

2. Mathematical model

The problem, a sandwich panel exposed to a hydrocarbon flame (schematic in Fig. 1, the thickness of the three zones is L_{S1}, L_{S2} and L_C, the width and length show the same size H), and the equations of the mathematical model (Tables 1A and 1B) are the same as already presented [1], so only the main features are briefly summarized here. The upper surface located at $x = 0$ is exposed to a hydrocarbon flame where the temperature is a known function of time (eqn. (50)). More precisely, the standard fire exposure is described according to the Norwegian Petroleum Directorate (NPD) [13]. At the heat-exposed surface heat transfer takes place by

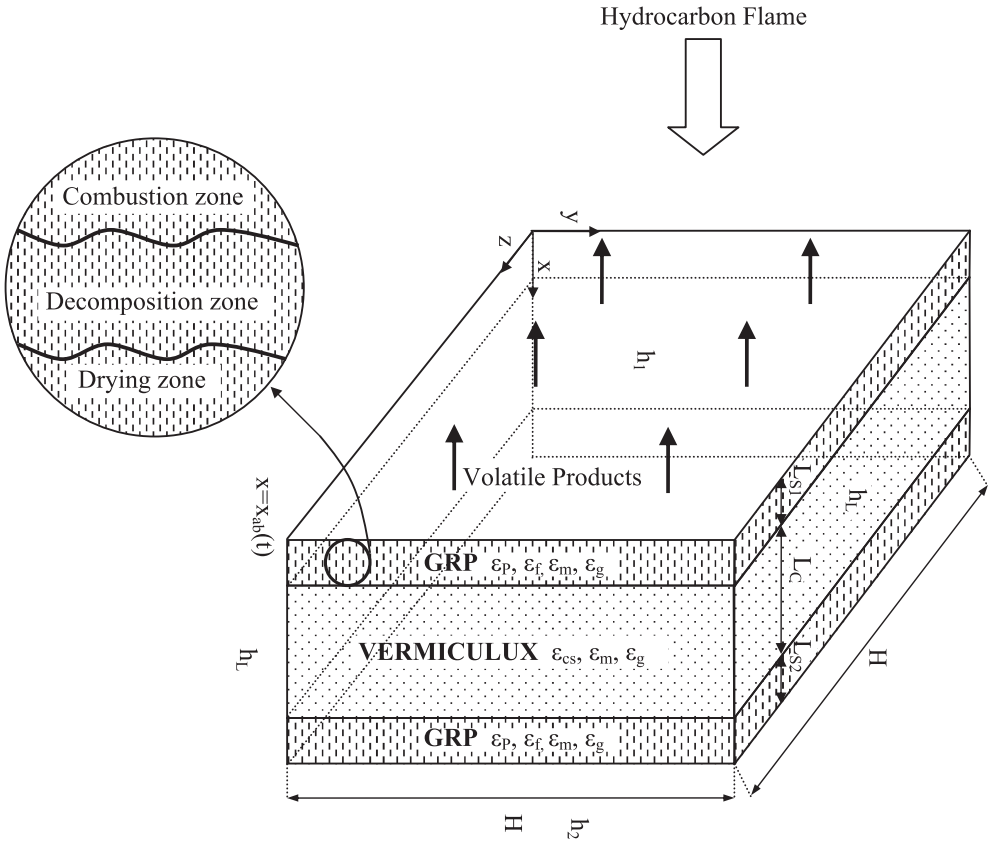

Fig. 1. Schematic of the GRP/Vermiculux sandwich panel.

Table 1A
Kinetic and transport equations.

Chemical reaction rate and drying rate

$$\omega_d = A_d \exp\left(-\frac{E_d}{RT}\right) Y_d, \tag{1}$$

$$\omega_c = A_c \exp\left(-\frac{E_c}{RT}\right) Y_c^n, \tag{2}$$

$$\omega_m = A_m \exp\left(-\frac{E_m}{RT}\right) Y_m \tag{3}$$

Transport equations for the skins
$(x_{ab}(t) < x < L_{S1}$ and $L_{S1} + L_C < x < L_{S1} + L_C + L_{S2})$

$$\frac{d}{dt} Y_d = -A_d \exp\left(-\frac{E_d}{RT}\right) Y_d \tag{4}$$

$$\frac{d}{dt} Y_c = -A_c \exp\left(-\frac{E_c}{RT}\right) Y_c^n \tag{5}$$

$$\frac{d}{dt} Y_m = -A_m \exp\left(-\frac{E_m}{RT}\right) Y_m \tag{6}$$

$$\frac{\partial}{\partial t}\varepsilon_g \rho_v - \alpha \frac{\partial}{\partial x} u \rho_v = \omega_m \rho_{S0}, \tag{7}$$

$$\frac{\partial}{\partial t}\varepsilon_g \rho_G - \alpha \frac{\partial}{\partial x} u \rho_G = (\omega_d + \omega_c)\rho_{S0} \tag{8}$$

$$\frac{\partial}{\partial t}\varepsilon_g \rho_g - \alpha \frac{\partial}{\partial x} u \rho_g = (\omega_d + \omega_c + \omega_m)\rho_{S0}, \tag{9}$$

$$\rho_g = \frac{pM}{RT} \tag{10}$$

$$\left(\varepsilon_m \rho_m c_m + \varepsilon_p \rho_p c_p + \varepsilon_f \rho_f c_f + \varepsilon_g \rho_g c_g\right)\frac{\partial}{\partial t} T - \alpha u \rho_g c_g \frac{\partial}{\partial x} T = \frac{\partial}{\partial x}\left(k_e \frac{\partial}{\partial x} T\right) + \omega_d \rho_{S0}(-\Delta H_1) + \omega_c \rho_{S0}(-\Delta H_2) - \lambda \omega_m \rho_{S0} + S\left[h_L(T_e - T) + \sigma e\left(T_e^4 - T^4\right)\right] \tag{11}$$

Transport equations for the core ($L_{S1} < x < L_{S1} + L_C$)

$$\frac{d}{dt} Y_m = -\omega_m, \tag{12}$$

$$\frac{\partial}{\partial t}\varepsilon_g \rho_v - \alpha \frac{\partial}{\partial x} u \rho_v = \omega_m \rho_{C0}, \tag{13}$$

$$\frac{\partial}{\partial t}\varepsilon_g \rho_G - \alpha \frac{\partial}{\partial x} u \rho_G = 0 \tag{14}$$

$$\frac{\partial}{\partial t}\varepsilon_g \rho_g - \alpha \frac{\partial}{\partial x} u \rho_g = \omega_m \rho_{C0}, \tag{15}$$

$$\rho_g = \frac{pM}{RT} \tag{16}$$

$$\left(\varepsilon_m \rho_m c_m + \varepsilon_{cs} \rho_{cs} c_{cs} + \varepsilon_g \rho_g c_g\right)\frac{\partial}{\partial t} T - \alpha u \rho_g c_g \frac{\partial}{\partial x} T = \frac{\partial}{\partial x}\left(k_e \frac{\partial}{\partial x} T\right) - \lambda \omega_m \rho_{C0} + S\left[h_L(T_e - T) + \sigma e\left(T_e^4 - T^4\right)\right] \tag{17}$$

Table 1B
Boundary conditions and equations for the physical properties.

Boundary conditions

$$-k_e \left.\frac{\partial T}{\partial x}\right|_{x=x_{ab}} = \psi \sigma e|_{x=x_{ab}} \left(T_f^4 - T^4|_{x=x_{ab}}\right) + h_1\left(T_f - T|_{x=x_{ab}}\right) \tag{18}$$

$$x_{ab}(t) = 0 \text{ for } T(0,t) = T_{cr} \quad \text{and} \quad x_{ab}(t) = x(T_{cr}) \text{ for } T(0,t) > T_{cr} \tag{19}$$

$$\rho_v|_{x=L_{S1}^-} = \rho_v|_{x=L_{S1}^+}, \tag{20}$$

$$\rho_G|_{x=L_{S1}^-} = \rho_G|_{x=L_{S1}^+}, \tag{21}$$

$$\alpha \rho_g u|_{x=L_{S1}^-} = \alpha \rho_g u|_{x=L_{S1}^+} \tag{22}$$

$$\rho_v|_{x=(L_{S1}+L_C)^-} = \rho_v|_{x=(L_{S1}+L_C)^+}, \tag{23}$$

$$\rho_G|_{x=(L_{S1}+L_C)^-} = \rho_G|_{x=(L_{S1}+L_C)^+}, \tag{24}$$

$$\alpha \rho_g u|_{x=(L_{S1}+L_C)^-} = \alpha \rho_g u|_{x=(L_{S1}+L_C)^+} \tag{25}$$

$$T|_{x=L_{S1}^-} = T|_{x=L_{S1}^+}, \tag{26}$$

$$k_e \left.\frac{\partial T}{\partial x}\right|_{x=L_{S1}^-} = k_e \left.\frac{\partial T}{\partial x}\right|_{x=L_{S1}^+}, \tag{27}$$

$$T|_{x=(L_{S1}+L_C)^-} = T|_{x=(L_{S1}+L_C)^+} \tag{28}$$

$$k_e \left.\frac{\partial T}{\partial x}\right|_{x=(L_{S1}+L_C)^-} = k_e \left.\frac{\partial T}{\partial x}\right|_{x=(L_{S1}+L_C)^+}, \tag{29}$$

$$\rho_v|_{x=L_{S1}+L_C+L_{S2}} = 0, \tag{30}$$

$$\rho_G|_{x=L_{S1}+L_C+L_{S2}} = 0, \tag{31}$$

$$\alpha \rho_g u|_{x=L_{S1}+L_C+L_{S2}} = 0 \tag{32}$$

$$-k_e \left.\frac{\partial T}{\partial x}\right|_{x=L_{S1}+L_C+L_{S2}} = \sigma e|_{x=L_{S1}+L_C+L_{S2}} \left(T^4|_{x=L_{S1}+L_C+L_{S2}} - T_e^4\right) + h_2\left(T|_{x=L_{S1}+L_C+L_{S2}} - T_e\right) \tag{33}$$

Single skin at the bottom side ($x = L_{S1}$)

$$\rho_v|_{x=L_{S1}} = 0, \tag{34}$$

$$\rho_G|_{x=L_{S1}} = 0, \tag{35}$$

$$\alpha \rho_g u|_{x=L_{S1}} = 0, \tag{36}$$

$$-k_e \left.\frac{\partial T}{\partial x}\right|_{x=L_{S1}} = \sigma e|_{x=L_{S1}} \left(T^4|_{x=L_{S1}} - T_e^4\right) + h_2\left(T|_{x=L_{S1}} - T_e\right) \tag{37}$$

Physical properties

$$\varepsilon_p + \varepsilon_f + \varepsilon_m + \varepsilon_g = 1 \text{ (skin)}, \tag{38}$$

$$\varepsilon_{cs} + \varepsilon_m + \varepsilon_g = 1 \text{ (core)}, \tag{39}$$

$$\frac{\varepsilon_p}{\varepsilon_{p0}} = \frac{Y_d + Y_c + Y_r}{Y_{d0} + Y_{c0} + Y_r} \tag{40}$$

$$\frac{\varepsilon_m}{\varepsilon_{m0}} = \frac{Y_m}{Y_{m0}} \tag{41}$$

$$k_{eS} = k'_e + 4d\frac{\varepsilon_g}{1 - \varepsilon_g}\sigma e T^3, \tag{42}$$

$$\frac{1}{k'_e} = \frac{\varepsilon_f}{k_f} + \frac{1 - \varepsilon_f}{k_{pgm}}, \tag{43}$$

$$k_{pgm} = \frac{\varepsilon_p}{1 - \varepsilon_f} k_p + \frac{\varepsilon_g}{1 - \varepsilon_f} k_g + \frac{\varepsilon_m}{1 - \varepsilon_f} k_m \tag{44}$$

$$e = 0.755 + 2.5 \times 10^{-4}(T - 293), \tag{45}$$

$$k_g = 9.00037 \times 10^{-3} + 5.6263 \times 10^{-5} T \text{ [W/mK]} \tag{46}$$

$$k_f = \frac{a_{kf1} + a_{kf2}(T - 293)^{a_{kf3}}}{1 + a_{kf4}(T - 293)^{a_{kf3}}} \text{ [W/mK]}, \tag{47}$$

$$k_{eC} = \varepsilon_{cs} k_{cs} + \varepsilon_m k_m + \varepsilon_g k_g + 4d\frac{\varepsilon_g}{1 - \varepsilon_g}\sigma e T^3 \tag{48}$$

(*continued on next page*)

convection (convective heat transfer coefficient h_1) and radiation. Sample radiative and convective heat losses with the environment at ambient temperature are also modelled along the later surfaces (the four surfaces with area $H \times (L_{S1} + L_C + L_{S2})$) with a convective heat transfer coefficient h_L and the bottom surface ($H \times H$) with a convective heat transfer coefficient h_2.

The unsteady, one-dimensional conservation equations are written using the porous medium approximation. The composite materials are treated as porous media consisting of a condensed phase and a gas/vapour phase. The condensed phase includes the solid-phase components (i.e. polymeric resin and glass fibres for the skins and Vermiculux for the core) and the liquid-phase moisture. Each condensed- or gas/vapour-phase component is described as a continuum in a global coordinate system. The model takes into account two-step, finite rate kinetics for the thermal decomposition and combustion of the polymeric resin (isophthalic polyester), moisture evaporation described by an Arrhenius rate

Table 1B (*continued*)

$$Nu = \left[0.825 + \frac{0.387Ra^{1/6}}{\left(1+\left(\frac{0.492}{Pr}\right)^{9/16}\right)^{8/27}}\right]^2, \quad (49)$$

$$T_f = 293 + 1080\left(1 - 0.325e^{-0.0028t} - 0.675e^{-0.042t}\right)\ [\mathrm{K}] \quad (50)$$

law, heat transfer by convection and conduction (the latter with theoretically based sub-models for the effective thermal conductivities), convective mass transfer, variation of the volumetric fractions of the polymeric resin and the moisture with the conversion degree, effective specific heats, convective and radiative heat losses from the lateral and bottom surfaces. Finally, surface ablation is also taken into account of the fibre glass layer, left at the conclusion of the chemical reactions, as soon as the temperature becomes higher than a critical value, T_{cr} (around 1200 K for glass fibres [1]), representative of the continuous depletion of mechanical strength of the glass fibres. The following main assumptions are made: no change in the total volume occupied by skins and core takes place as a consequence of moisture evaporation and oxidative decomposition; the core does not shrink or swell and is chemically inert; the gas pressure inside the pores of the sandwich is constantly at the atmospheric value; the solid, liquid and the gas/vapour phases are in a local thermal equilibrium, the diffusion of volatile species is small with respect to convection, convection and diffusion of the liquid-phase moisture are negligible, the gaseous mixture obeys to the ideal gas law. The validity of these assumptions is already discussed in [1] and for some of them an analysis is carried out here. It is just worth recalling that these are, for a large part, usually made in the formulation of transport equations for porous reacting solids (see the references cited in [1]), in particular the validity of the ideal gas law, or are specific for the system modelled, in particular the core properties.

The model equations consist of the kinetic laws (eqns. (1)–(3)), the mass conservation equations (eqns. (4)–(10)) and the enthalpy equation (eqn. (11)) for the skins and also the transport equations for the mass (eqns. (12)–(16)) and the enthalpy (eqn. (17)) for the core (Table 1A). Boundary conditions and equations for physical properties and global coefficients are listed in Table 1B. The model equations for the single skin panel are the same as already presented with the sole variation in the boundary conditions at the bottom side where eqns. (20)–(22) are substituted by eqns. (34)–(37). The set of intrinsic property values, all available or estimated from experimental measurements and already used in [1], are listed in Table 2. The simulation results obtained by means of the model equations reported in Tables 1A and 1B and the input data of Table 2 are used as a reference for the sensitivity analysis of the model to assumptions and input parameter values.

Table 2
Physical property values.

Parameter	Value	Reference
a_{kf1}	1.1 [W/mK]	[1]
a_{kf2}	2.7×10^{-17} [W/mK^7]	[1]
a_{kf3}	6	[1]
a_{kf4}	7.0×10^{-18}	[1]
A_m	5.6×10^8 [s^{-1}]	[14]
c_a	1100 [J/kg K]	[15]
c_{cs}	950 [J/kg K]	[16]
c_f	840 [J/kg K]	[17]
c_G	2500 [J/kg K]	[15]
c_m	4200 [J/kg K]	[18]
c_p	2500 [J/kg K]	[19]
c_v	2100 [J/kgK]	[18]
d	3.0×10^{-4} (skin) [m]	[19]
	2.0×10^{-5} (core) [m]	[16]
E_m	88 [kJ/mol]	[14]
k_{cs}	0.77 [W/mK]	[16]
k_m	0.23 [W/mK]	[20]
k_p	0.31 [W/mK]	[19]
M_G	95 [kg/kmol]	[21]
M_a	29 [kg/kmol]	[18]
M_v	18 [kg/kmol]	[18]
T_{cr}	1200 [K]	[1]
α	1.0	[1]
ε_{cs}	0.172	[22,18]
ε_f	0.465	[23]
ε_{g0}	0.15 (skin)	[24]
	0.773 (core)	[12,22,18]
ε_{m0}	0.018 (skin)	[12]
	0.055 (core)	
ε_{p0}	0.367	[23]
γ_0	6.18×10^{-18} [m^2]	[24]
γ_c	4.85×10^{-15} [m^2]	[24]
γ_r	4.85×10^{-15} [m^2]	Guessed
λ	2.26×10^6 [J/kg]	[18]
ρ_{cs}	2900 [kg/m^3]	[18]
ρ_f	2560 [kg/m^3]	[23]
ρ_p	1749 [kg/m^3]	[23]
ψ	0.7	[25]

2.1. Modifications of the mathematical model

To examine the impact of the approach used in the description of various processes on the predicted dynamics of the composite structure exposed to a hydrocarbon flame, several versions of the reference model presented in Tables 1A and 1B should be considered. The following aspects are examined:

a) models of external heating and heat transfer between the lateral and bottom surfaces of the structure and the environment;
b) mathematical description of the heat transfer rate between the condensed phase and the volatile products, one-step (decomposition) or two-step (decomposition and combustion) kinetics for polymer conversion, thermal versus oxidative decomposition of the polymer, moisture evaporation;
c) models of the effective thermal conductivity for the skins;
d) mathematical description of variations in the pressure of the gas flowing through the pores of the panel.

2.1.1. a) Models of external heating and heat transfer between the lateral and bottom surfaces of the structure and the environment

Simulation results, obtained by means of the reference model [1] show that the heating and conversion dynamics of the multi-layered structure are affected by both the intensity of the externally applied heat flux and the distance between the heat-exposed surface and the position of the evaporation/reaction zone. Therefore the effects of surface ablation, external heat transfer resistance, surface heat losses and different standard fire exposures are investigated.

The reference model without the description of the ablation of the surface is indicated with the acronym NA (No Ablation). It is obtained by substituting eqn. (19) of Table 1B with

$$x_{ab}(t) = 0, \quad \text{for } t > 0 \quad (51)$$

This analysis is important for the implications of the ablation process on the fire behaviour of complex structures. Moreover it is also useful for understanding whether the description of surface ablation can be neglected, for ablating materials, in the mathematical description of multi-layered systems subjected to fire.

A comparison is also made with the reference model, which includes an external heat transfer resistance (eqn. (18)) in the description of the heat transfer from the NPD temperature curve (eqn. (50)), and a model which assumes that the surface is instantaneously at the NPD (flame) temperature, again with and without surface ablation. These two models are indicated with the acronyms NHR (No external Heat transfer Resistance) and NHRNA (No external Heat transfer Resistance and No Ablation), respectively. More precisely, eqn. (18) is substituted by eqns. (52) and (53), respectively:

$$T|_{x=x_{ab}} = T_f(t), \tag{52}$$

$$T|_{x=0} = T_f(t) \tag{53}$$

It is understandable that the exposure of a composite material to an external heat flux is, from the physical point of view, accompanied by the existence of a resistance to heat transfer. Thus, the examination of this model feature is useful for understanding whether a simplification in the treatment of the boundary conditions is feasible.

Also, to quantify the magnitude of the surface heat losses, simulations are carried out for the two cases of adiabatic lateral and bottom surfaces. These, respectively, correspond to the heat exchange contribution in the enthalpy conservation equations ((11) and (17)) assumed to be zero and to the substitution of equation (33) with eqn. (54):

$$-k_e \frac{\partial T}{\partial x}\bigg|_{x=L_{S1}+L_C+L_{S2}} = 0 \tag{54}$$

In this case, when a single skin panel is considered, the condition of adiabatic bottom surface is expressed by substituting eqn. (37) with eqn. (55):

$$-k_e \frac{\partial T}{\partial x}\bigg|_{x=L_{S1}} = 0 \tag{55}$$

These two cases are indicated with the acronyms ALS (Adiabatic Lateral Surface) and ABS (Adiabatic Bottom Surface), respectively.

In real scale systems, heat losses from the surfaces not exposed to the heat flux can be quite large. However, these are often disregarded in the related mathematical models. Hence, it can be useful to quantify these influences by comparing the results of the reference model, based on reasonable values for global heat transfer coefficients, with the case of perfectly adiabatic boundaries. The convective heat transfer coefficients h_1 and h_2 (upper and bottom surface, respectively) are evaluated using the correlation for the Nusselt number given by eqn. (49) and valid for vertical plates. All the properties are evaluated at the film temperature as mean values between the surface and the ambient temperature. The surface temperature is assumed to be 1273 K for the computation of h_1 and 433 K for h_2 [1]. The lateral heat transfer coefficient h_L is the average of the h_1 and h_2 values, before the former is modified to take into account the blowing effect [1].

The intensity of the externally applied heat flux to be used for structure design depends on the legislative environment and the design philosophy [26]. In addition to the NPD standard used by the reference model (eqn. (50)), two other standards are also examined which are indicated as ISO834 and ASTM E119 [13,26]. The flame temperature for the two cases expresses as:

$$T_f = 293 + 345 \log_{10}(0.133t + 1) \tag{56}$$

$$T_f = 293 + 1080\left(1 - 0.676e^{-0.0033t} - 0.324e^{-1.67\times10^{-4}t}\right) \tag{57}$$

(the latter equation results from a fitting procedure of experimental data assuming that the maximum temperature value is the same as for the NPD curve, that is, 1373 K). Fig. 2 compares the flame temperatures as predicted by the three standard fire exposures.

Although the high flammability and poor fire resistance of sandwich composite in marine structures is well recognized [10], there are no generally accepted fire standards. Therefore, it can be interesting to quantify, by means of numerical simulation, the modifications induced in the predictions by the different standards.

2.1.2. b) Heat transfer rate between the condensed phase and the volatile products

All the models of composite material degradation, but one [8], assume that convective heat and mass transport take place under conditions of thermal equilibrium owing to micro-porosity. However, practical situations, possibly also as a consequence of structural failure, may deviate from this assumption. Hence an analysis is carried out motivated by the need to quantify the differences in the process predictions induced by such deviations.

The importance of the heat transfer rate between the condensed phase and the gas/vapour phase is analyzed by means of the contributions due to convective heat and mass transfer in the conservation equations for the enthalpy and the gas/vapour phase species for both skin and core (eqns. (7)–(9), (11), (13)–(15), (17)). For the reference case it is $\alpha = 1$, corresponding to the assumption that all the volatile species produced are released at the heat-exposed surface and are at the same temperature as the condensed phase. Two additional situations are examined here, that is, the volatile products of moisture evaporation and polymer conversion are completely ($\alpha = 0$) or in part (the half, $\alpha = 0.5$) released at the location where they are generated (the acronyms used for these two models are NHCG (No Heat transfer between Condensed and Gas phase) and PHCG (Partial Heat transfer between Condensed and Gas phase), respectively). In other words, there is no ($\alpha = 0$), partial ($\alpha = 0.5$) or total ($\alpha = 1$) heat exchange between the condensed phase and the volatile products, in this way describing the effects of changes in the level of local thermal equilibrium. These simulations are not associated with modifications in the model structure but simply with variation in the input parameter α whose range of values spans all the physically possible situations.

The role played by the heat and volatile amounts absorbed/generated from moisture evaporation and polymer combustion is also examined. The motivation of this analysis stems from the usual assumptions [2,3] that polymer conversion can be described by

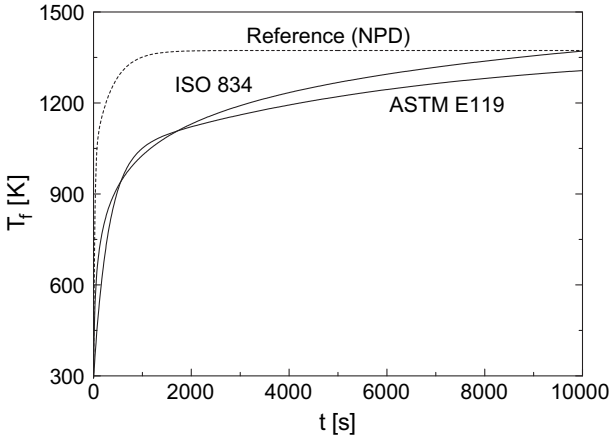

Fig. 2. Time profile of the flame temperature, T_f, as predicted (eqns. (50), (56), and (57)) by three fire exposure standards [13,26].

a one-step global reaction (instead of the two-step mechanism of Ref. [1]) and moisture evaporation can be neglected, that is, only a small amount of polymer undergoes combustion and the initial moisture content is generally below 1–10% [1]. However, the quantitative effects of these assumptions on the simulation results are not known. These two models are indicated with the acronyms NC (No Combustion) and NM (No Moisture), respectively. Finally, as in the presence of gas phase combustion, the flame could act as a physical barrier [27] hindering the oxygen access to the site of the heterogeneous reactions, the one-step kinetics for the thermal degradation (versus oxidative decomposition of the reference model) of isophthalic polyester, as determined in [27] ($E = 134$ kJ/mol and $A = 1.15 \times 10^8$ s^{-1}), are also examined. This model is indicated with the acronym TD (Thermal Decomposition). Also, for these simplifications there are no modifications in the model structure but simply in the input parameters.

2.1.3. c) Models of the effective thermal conductivity

The solid-phase thermal conductivities are important parameters in the predictions of the high-temperature response of combustible materials [2,25]. The reference model (Tables 1A and 1B) for the composite material skin is based on the assumption that the system polymer-moisture, on one side, and gas-vapour, on the other, can be described by a spatially parallel mechanism where the contribution of the components is weighted in proportion to the respective volumetric fraction (eqn. (44)). A similar treatment is also applied for the porous material of the core (eqn. (48) of Table 1B). More complicated, in the case of the skins, is the description of the interaction between the porous polymeric system and the glass fibres. The reference model (eqn. (43)) assumes a series model.

In reality, many (if not most) of the models for the effective thermal conductivity of heterogeneous or composite materials are generally based on one or more of five basic structural models, that is, the Series (S), Parallel (P), Maxwell–Eucken (two forms, ME1 and ME2) and Effective Medium Theory (EMT) models [28,29] (acronyms are used in the following to indicate the various models). The physical assumptions lying behind the S and P models are that layers of components are aligned either perpendicular or parallel to the heat flow. The Maxwell–Eucken model describes a dispersion of small non-interacting spheres within a continuous matrix of a different component. For a two-component material, two forms of the Maxwell–Eucken model are proposed depending on which of the components forms the continuous phase: ME1 (fibres) and ME2 (polymer). The EMT model assumes a completely random distribution of all the components. In this analysis, the performances of the P model, the two forms of the Maxwell–Eucken model (ME1, ME2) and the EMT model for the description of the interactions between the porous polymer (always modelled with a P model) and the glass fibres are compared with the S model of the reference case. The comparison is made for both the skin and the sandwich panels using the same parameter values as reported in Table 2. The model equations for the effective thermal conductivities, indicated as above, are:

$$k'_e = k_f\varepsilon_f + k_{pgm}\left(1-\varepsilon_f\right) \quad \text{(P)} \tag{58}$$

$$k'_e = k_{pgm}\frac{2k_{pgm} + k_f - 2\left(k_{pgm}-k_f\right)\varepsilon_f}{2k_{pgm} + k_f + \left(k_{pgm}-k_f\right)\varepsilon_f} \quad \text{(ME1)} \tag{59}$$

$$k'_e = k_f\frac{2k_f + k_{pgm} - 2\left(k_f-k_{pgm}\right)\left(1-\varepsilon_f\right)}{2k_f + k_{pgm} + \left(k_f-k_{pgm}\right)\left(1-\varepsilon_f\right)} \quad \text{(ME2)} \tag{60}$$

$$\left(1-\varepsilon_f\right)\frac{k_{pgm}-k'_e}{k_{pgm}+2k'_e} + \varepsilon_f\frac{k_f-k'_e}{k_f+2k'_e} = 0 \quad \text{(EMT)} \tag{61}$$

2.1.4. d) Variable pressure model

The fast and significant rate of volatile formation from moisture evaporation and decomposition of the polymeric part of the composite material can give rise to significant variations in the gas pressure, with respect to the atmospheric value, which can be described according to the Darcy law (eqn. (62)):

$$u = -\frac{\gamma}{\mu}\frac{\partial p}{\partial x} \tag{62}$$

where the permeability to gas flow, γ, is assumed to vary with the conversion level (skin, eqn. (63)) or to be constant (core, eqn. (64)):

$$\gamma = (1-\eta)\gamma_0 + \eta\gamma_r, \tag{63}$$

$$\gamma = \gamma_c, \tag{64}$$

$$\eta = 1 - \frac{Y_d + Y_c}{Y_{d0} + Y_{c0}} \tag{65}$$

Permeability values, γ_0, γ_r and γ_c, are listed in Table 2. The gas phase viscosity, μ, is linearly dependent on temperature [18,30]:

$$\mu = 7.87 \times 10^{-6} + 3.74 \times 10^{-8}T \ \text{[Pa s]} \tag{66}$$

At the externally heated surface the pressure is at the atmospheric value whereas the bottom surface is assumed to be an impermeable barrier. Thus the boundary conditions for the sandwich panel are expressed as:

$$p|_{x=x_{ab}} = p_{atm}, \tag{67}$$

$$\left.\frac{\partial p}{\partial x}\right|_{x=L_{S1}+L_C+L_{S2}} = 0 \tag{68}$$

(the same conditions apply at the upper and bottom side, respectively, of the single skin panel).

Equations (62)–(68) with those listed in Tables 1A and 1B allow the pressure to be computed, following the approach already used in previous models [2,31] for charring solid pyrolysis. This model is indicated in the following discussion as VP (Variable Pressure) model.

The reference model assumes that the gas pressure remains constant at the atmospheric value while the gas velocity is obtained from the integral, over the sample thickness, of the rate of volatile species production. Given the significant complication in the mathematical model introduced by the Darcy law, it is certainly relevant to ascertain via numerical simulation the impact on the system thermal response exerted by linking pressure and velocity variations.

3. Results

Results are presented describing the influences exerted by the mathematical descriptions of the problem outlined at points a)–d) of the previous section on the predictions of process dynamics using the input data listed in Table 2 and the results of the reference model (Tables 1A and 1B) for comparison. Finally results are presented of a sensitivity analysis to the main input parameters.

In general, the spatial profiles at several instants of the main dependent variables are examined mainly with the scope of putting into evidence the changes induced by the various model

simplifications/assumptions on the predicted characteristics of the process. The temperature versus time predictions are compared with experimental data at $x = L_{S1}/2$ for the single skin panel and the cold bottom side ($x = L_{S1} + L_C + L_{S2}$) for the sandwich panel. Particular attention is given to the latter since it is useful for the standard fire test H120 requiring a time not shorter than 120 min to reach a temperature of 433 K [12]. In the following, to discuss quantitatively the process dynamics, several characteristic times are used. They are defined as: t_{625}, the time needed to achieve a temperature of 625 K at the centre of the upper skin, t_{ds1}, the drying time of the upper skin, t_{a1} and t_{a2}, the times corresponding to the beginning and conclusion of surface ablation, t_c, the conversion time for the upper skin, t_{750} the time needed to achieve a temperature of 750 K at the centre of the core, t_{dc}, the time of core drying and t_{ds2}, the drying time of the lower skin (the times introduced for the upper skin of the sandwich also apply to the single skin panel). Drying and conversion times refer to total mass fractions of the moisture content and the polymeric fraction reduced to 10%.

Before analyzing the results it is import to recall that the simulated dynamics [1] of the sandwich structure for the reference case are highly influenced by the behaviour of the heat-exposed skin which shows three main regimes: I) very rapid conversion from virgin resin to char and volatiles of a thin surface layer (fast heating regime), II) slowing down of the conversion processes following the formation of a thick insulating fibre glass layer (slow heating regime) and III) a new enhancement in the reaction rates as a consequence of surface collapse and ablation (ablation regime). Temperature gradients along the core thickness are quite high (up to about 25,000 K/m). Hence, after moisture evaporation, the temperatures of the bottom skin are too low (below 500 K) and the activity of chemical reactions is completely hindered. On the other hand, the dynamics of the upper skin do not appear to be significantly influenced by the core layer.

3.1. Model sensitivity to assumptions

3.1.1. Models of external heating and heat transfer between the lateral and bottom surfaces of the structure and the environment

Results obtained with the models removing the ablation of the heat-exposed surface, the external heat transfer resistance and the lateral and bottom heat losses are discussed in this section. Figs. 3 and 4 and Table 3 refer to the single skin panel case. More precisely, Fig. 3 reports an example of the spatial temperature profiles at several times as simulated with the reference model (Tables 1A and 1B, dashed lines) and the same model but in the absence of surface ablation (NA, solid lines). As expected, differences appear only for times longer that 630 s (beginning of surface ablation, corresponding to surface temperatures of 1200 K). The presence of a progressively thicker inert layer, as a consequence of the decomposition reactions and the absence of surface ablation, delays solid heating (temperature differences up to 500–600 K) and the occurrence of chemical reactions.

Fig. 4A and B shows the temperature versus time profiles at $x = L_{S1}/2$ as simulated for the cases of 1) an adiabatic lateral surface (ALS), 2) an adiabatic bottom surface (ABS), 3) the absence of surface ablation (NA), 4) the absence of external heat transfer resistance with (NHR) and without (NHRNA) surface ablation and 5) the flame temperature modelled according to the three standards introduced above (the experimental measurements [32] are included for comparison purposes). It can be observed that the effects associated with the lateral and bottom heat losses are negligible with an almost perfect coincidence between the assumption of an adiabatic wall and the results of the reference model. This is the result of a small lateral heat transfer coefficient (about 8.5 W/m^{2}K) and the fast

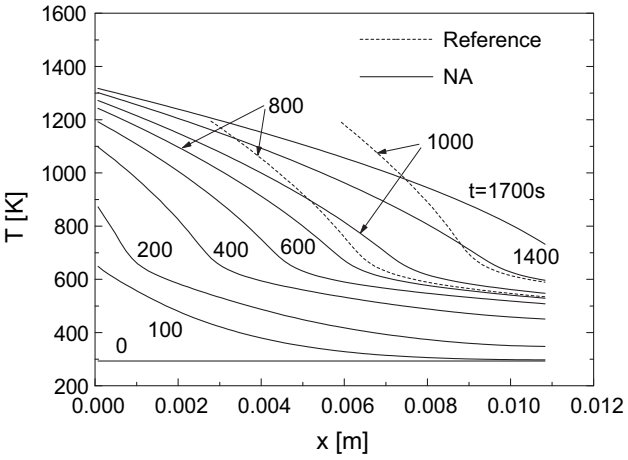

Fig. 3. Temperature profiles along the single skin panel for several times as predicted by the reference model ([1], dashes lines) and in the absence of surface ablation (NA, solid lines).

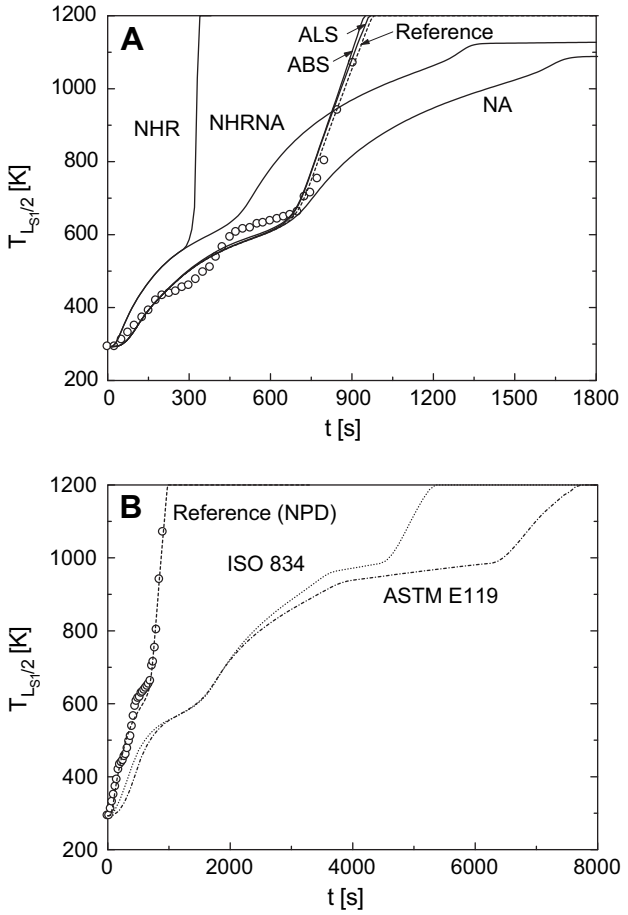

Fig. 4. Predicted (lines) and measured ([32], symbols) temperatures versus time profiles at $x = L_{S1}/2$ for the single skin panel. A: Predictions are obtained with the reference model [1] (dashed lines) and the assumptions of adiabatic bottom surface (ABS), adiabatic lateral surface (ALS), absence of surface ablation (NA), no external heat transfer resistance (NHR) also in the absence of surface ablation (NHRNA). B: Predictions are obtained with the reference model [1] and the NPD (dashed line), ISO834 (dotted line) and ASTM E119 (dashed-dotted line) exposure standards.

Table 3
Characteristic times of the single skin panel as predicted with the various models and percentage variations with respect to the predictions of the reference model [1]: t_{625}, time needed to achieve a temperature of 625 K at the centre of the skin, t_{ds1}, drying time, t_{a1} and t_{a2}, times corresponding to the beginning and conclusion of surface ablation, t_c, conversion time (acronyms as in Figs. 4, 9, 12 and 15 and Nomenclature).

	Model	t_{625} [s]; %	t_{ds1} [s]; %	t_{a1} [s]; %	t_c [s]; %	t_{a2} [s]; %
	Reference	644	358	626	1022	1120
a	ABS	628; −2.6	336; −6.0	630; 0.7	951; −7.0	1023; −8.6
	ALS	636; −1.2	356; −0.3	615; −1.7	1008; −1.4	1105; −1.4
	NA	645; 0.1	358; 0.0	–	1321; 29.2	–
	NHR	312; −51.6	263; −26.4	271; −56.7	373; −63.5	375; −66.5
	NHRNA	436; −32.4	263; −26.4	–	1032; 0.9	–
	ISO834	1616; 151	584; 63.3	4467; 614	2843; 178	8723; 679
	ASTM E119	1602; 149	680; 90.1	6292; 906	2918; 185	16570; 1379
b	PHCG	608; −5.6	354; −0.9	594; −5.0	958; −6.3	1050; −6.3
	NHCG	571; −11.4	350; −2.0	563; −10.0	891; −12.9	1041; −7.1
	NC	704; 9.3	363; 1.4	650; 3.9	1106; 8.2	1235; 10.3
	TD	516; −20.0	331; −7.4	642; 2.7	1185; 15.9	1244; 11.1
	NM	633; −1.8	–	620; −0.8	1014; −0.8	1115; −0.4
c	ME1	553; −14.2	304; −15.0	683; 9.2	955; −6.6	Residue 10.8%
	EMC	458; −28.9	284; −20.6	830; 32.7	785; −23.2	Residue 20.0%
	ME2	433; −32.7	272; −23.9	810; 29.5	713; −30.3	Residue 28.4%
	P	422; −34.5	257; −28.0	782; 25.1	678; −33.7	Residue 33.3%
d	VP	644;−0.1	358; 0.0	624; −0.2	1020; −0.2	1116; −0.4

conversion rate of the polymeric resin over a relatively thin region (that is, conversion takes place in the presence of large spatial gradients of temperature and density along the skin thickness) well before high temperatures are attained at the bottom of the skin. The predictions obtained with the external upper surface instantaneously at the flame temperature in the presence of surface ablation (NHR) are qualitatively similar to those of the reference model. From the quantitative point of view, the actual heating conditions are much more severe, as testified by the significant anticipation of surface ablation (at about 270 s versus 630 s) and the higher temperatures (up to 80 K). On the other hand, the predictions obtained with the same boundary conditions but in the absence of surface ablation (NHRNA) are also characterized by temperatures higher (up to 200 K) than those of the corresponding case of the reference model. In other words, the presence of an external heat transfer resistance is always important (with or without surface ablation). The best agreement with the measurements is observed for the results of the reference model and those assuming adiabatic external surface as these do not induce significant changes in the predicted process features, that is, on the spatial profiles of the main variables at various instants. This finding confirms the correctness of the assumptions and mathematical description of the various processes made by the reference model.

Results in terms of characteristic times and deviations with respect to the predictions of the reference model (Table 3) confirm that the assumptions about the effects of lateral cooling and adiabatic bottom surface are small (below 2% for the former and between 1 and −9% for the latter). The removal of the ablation process from the reference model only affects the conversion time which is increased by about 30%. The removal of the external heat transfer resistance exerts a large influence on all the characteristic times. These are reduced by about 26–66% for the NHR model and about 1–32% for the NHRNA model.

The temperature profiles (Fig. 4B) and the characteristic times (Table 3) are dramatically influenced by the external flame temperature profile. In accordance with the temperature values (Fig. 2 and eqns. (50), (56) and (57)), the NPD standard predicts the fastest process. Differences between the other two are small for times shorter than approximately 3000 s. Then, given the higher T_f values, the ISO834 standard leads to a more rapid conversion process. Modifications in the characteristic process times, with respect to the reference model (NPD standard), are between 63–679% (ISO834) and 90–1379% (ASTM E119).

The effects of the assumptions about the external heat transfer modalities and models on the predicted dynamics of the sandwich panel are summarized by Figs. 5–8 and Table 4. Fig. 5 shows the spatial temperature profiles at several times for the model with adiabatic bottom side (ABS, solid lines) and the reference case (dashed lines) whereas Figs. 6 and 7 show the spatial profiles of the decomposition and combustion rates across the lower skin, at several times, as simulated for the case of adiabatic bottom surface. Fig. 8A and B reports the temperature versus time profiles at the bottom side ($x = L_{S1} + L_C + L_{S2}$) as simulated for the same cases as Fig. 4 and a further case assuming an adiabatic bottom surface and the absence of the combustion step (ABSNC) (experimental measurements [12] are included for comparison purposes). The effects associated with the absence of lateral heat losses (ALS), external surface temperature equal to the flame temperature and absence of ablation (NHR, NA, NHRNA) are qualitatively the same as discussed for the single panel case although they are quantitatively different, owing to the large thermal resistance offered by the core. The assumptions concerning the boundary conditions at the heat-exposed surface (NHR, NA, NHRNA) are important and cause a diminution in the characteristic times of about 29–72% (NHR) and 0–36% (NHRNA). It is worth noting that the large anticipation in the time of solid heating for the ablation process of the NHR model, when the temperature of the core layer is still low, highly affects the drying times (reduced by about 61%) which, instead, are left unchanged when ablation is not modelled. Compared with the single skin panel, the effects of adiabatic lateral surface become larger (t_{750} and t_{ds2} reduced by 31 and 19%, respectively). The absence of surface ablation for the reference case causes an increase in the conversion time of about 15% and much lower temperatures along the core layer which, at its centre, never reaches a temperature of 750 K. Modifications in description of the heating of the upper external surface (NHR, NA, NHRNA) also alter the thermal response of the sandwich in relation to the H120 test (Fig. 8A, Table 4).

Very large effects in terms of process dynamics are observed for the case of adiabatic bottom surface for times longer than those of the final steady solution of the reference case and are confined to

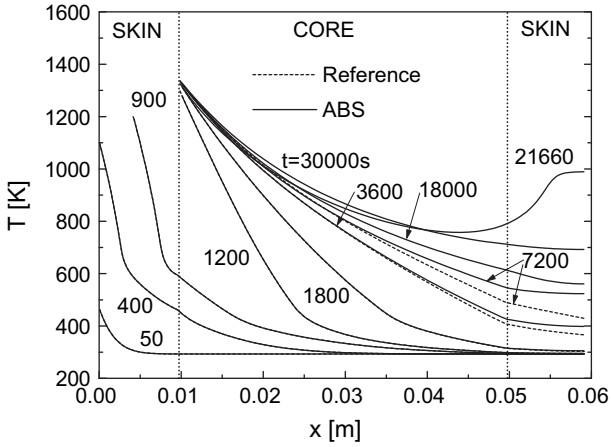

Fig. 5. Temperature profiles along the sandwich panel for several times as predicted by the reference model ([1], dashes lines) and with the assumption of adiabatic bottom surface (solid lines, ABS).

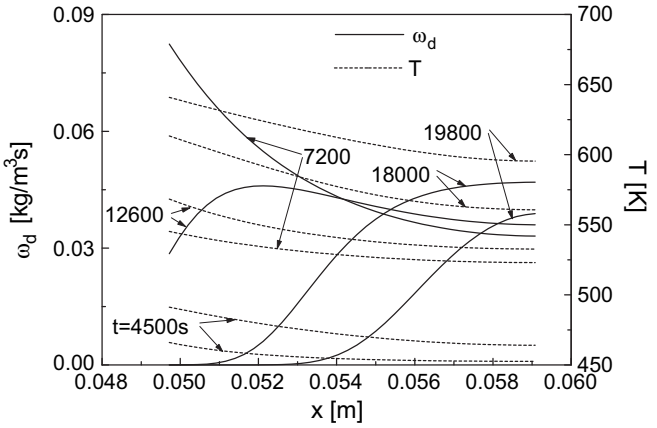

Fig. 6. Temperature (dashed lines) and decomposition rate (solid lines) profiles along the sandwich panel for several times as predicted by the model with the assumption of adiabatic bottom surface (ABS).

the bottom skin, so that the characteristic times collected in Table 4 are left almost unchanged. Indeed, contrary to the reference case, at very long times (>7200 s), the lower skin is slowly heated to temperatures which first cause complete decomposition and then combustion. In particular, temperatures attain peak values by far higher than the typical values of the reference case (Fig. 8A). The low-thermal conductivity and thick core make the heat transfer from the external applied flame to the lower skin very slow. Therefore, the decomposition rates, although they initially attain the highest values near the core/skin interface, are significant along the entire skin thickness (Fig. 6). As long as decomposition is underway, despite the endothermic character of the process, the temperature continuously increases, owing to the transfer from the heat-exposed core surface (the upper skin has already been completely ablated) and the adiabatic condition at the bottom skin. Once decomposition is terminated, the slightly higher temperatures at the bottom (variations of about 20 K along the core thickness) are further increased as a consequence of the beginning of the combustion reaction (Fig. 7). Owing to the exothermicity of the combustion process and the quite large thickness of the reaction zone (see the profiles of the combustion rate in Fig. 7) that propagates from the bottom towards the upper boundary of the skin, the temperature rapidly reaches maximum values up to about 1000 K

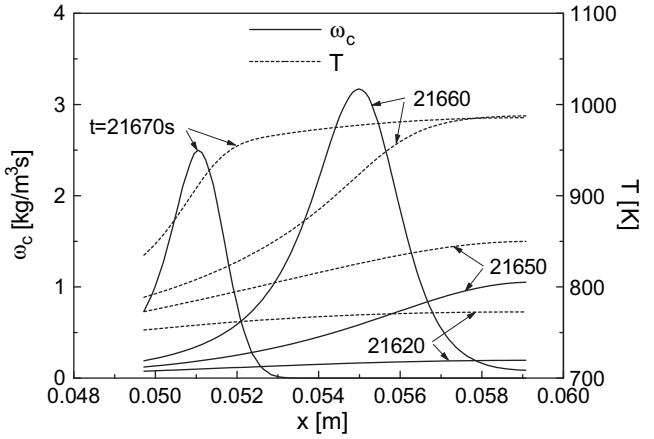

Fig. 7. Temperature (dashed lines) and combustion rate (solid lines) profiles along the sandwich panel for several times as predicted by the model with the assumption of adiabatic bottom surface (ABS).

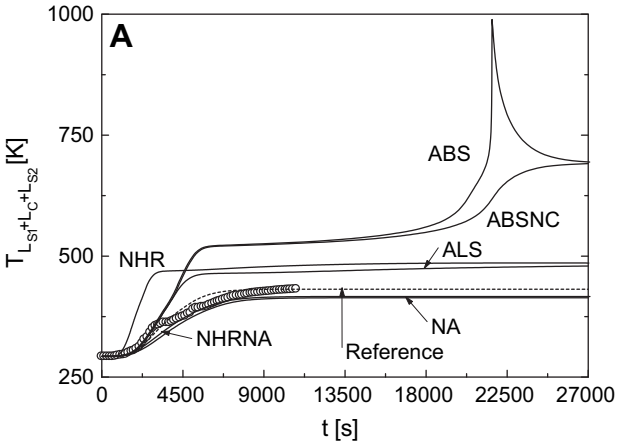

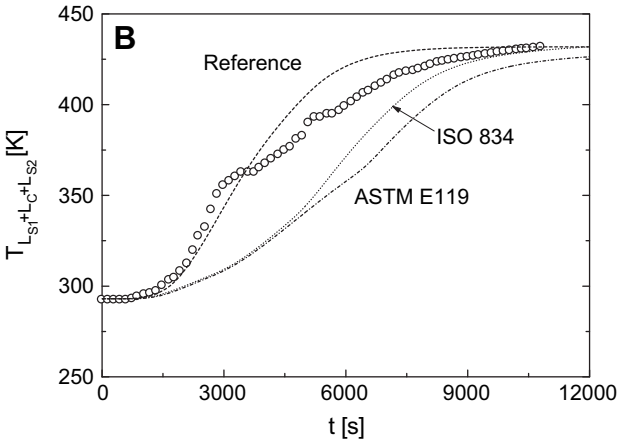

Fig. 8. Predicted (lines) and measured ([12], symbols) temperatures versus time profiles at $x = L_{S1} + L_C + L_{S2}$ for the sandwich panel. A: Predictions are obtained with the reference model [1] (dashed line) and the models ABS, ALS, NA, NHR, NHRNA (acronyms as in Fig. 4A) and adiabatic bottom surface in the absence of the combustion step (ABSNC). B: Predictions are obtained with the reference model [1] and the NPD (dashed line), ISO834 (dotted line) and ASTM E119 (dashed-dotted line) exposure standards.

(Figs. 7 and 8A). These high temperatures can be considered representative of heterogeneous ignition, that is, by the onset of smouldering combustion of the solid phase. It is important, however, to point out that this process is possible only when an adiabatic condition at the bottom side is applied, that is, the heat losses from the lateral surface are not sufficient to establish the profile of low-temperature values observed for the reference case. However, in the absence of the combustion reaction, the maximum value is around 650 K (Fig. 8A), which coincides with the final steady values reached once complete burn-out has been attained (as expected, the H120 test is never verified). In reality, a perfect adiabatic bottom wall is a limit condition, which is hardly achieved in practical situations. However, these findings point out the importance of establishing proper surface heat transfer conditions for multi-layered systems in order to guarantee fire resistance and safety conditions for the structure and the confining environment.

The effects of the simulated standard fire exposure laws on the predicted process dynamics (Fig. 8B, Table 4) are qualitatively similar to those already discussed for the single panel case but quantitatively lower. Indeed, compared with the reference (NPD) case, the characteristic times become longer by 49–540% (ISO834) and 65–774% (ASTM E119).

Table 4
Characteristic times of the sandwich panel as predicted by the various models and percentage variations with respect to the predictions of the reference model [1]: t_{625}, time needed to achieve a temperature of 625 K at the centre of the upper skin, t_{ds1}, drying time of the upper skin, t_{a1} and t_{a2}, times corresponding to the beginning and conclusion of surface ablation, t_c, conversion time for the upper skin, t_{750}, time needed to achieve a temperature of 750 K at the centre of the core, t_{dc}, drying time for the core and t_{ds2}, drying time of the bottom skin (acronyms as in Figs. 4, 9, 12 and 15 and Nomenclature).

	Model	H120	t_{625} [s]; %	t_{ds1}[s]; %	t_{750} [s]; %	t_{dc} [s]; %	t_{ds2} [s]; %	t_{a1} [s]; %	t_c [s]; %	t_{a2} [s]; %
	Reference	Yes	571	323	3165	2732	4762	631	934	1019
a	ABS	No	571; 0.0	323; 0.0	3240; 2.4	2702; −1.1	3942; −17.2	631; 0.0	934; 0.0	1018; −0.1
	ABSNC	No	627; 9.8	328; 1.3	3230; 2.1	2776; 1.6	4015; −15.7	654; 3.6	1003; 7.4	1115; 9.4
	ALS	No	565; −1.0	322; −0.3	2188; −30.9	2468; −9.7	3860; −18.9	621; −1.5	921; −1.4	1003; −1.6
	NA	Yes	571; 0.0	323; 0.0	–	3472; 27.0	6167; 29.5	–	1075; 15.1	–
	NHR	No	296; −48.2	231; −28.6	755; −72.4	1245; −60.7	2257; −52.6	270; −57.2	355; −62.0	358; −64.8
	NHRNA	Yes	367; −35.6	231; −28.6	–	3173; 0.2	5752; 20.8	–	831; −11.0	–
	ISO834	Yes	1438; 152	542; 67.8	7295; 130	4825; 76.6	7081; 48.7	4034; 540	2169; 132	4448; 336
	ASTM E119	Yes	1430; 151	639; 97.7	7620; 141	5024; 83.9	7833; 64.5	5512; 774	2187; 134	6023; 491
b	PHCG	Yes	537; −6.0	320; −1.0	2923; −7.6	2604; −4.7	4588; −3.6	596; −5.4	873; −6.5	951; −6.7
	NHCG	Yes	502; −11.9	317; −2.0	2672; −15.6	2468; −9.7	4405; −7.5	561; −11.0	805; −13.8	872; −14.4
	NC	Yes	627; 9.8	328; 1.3	3240; 2.4	2807; 2.7	4836; 1.6	654; 3.6	1003; 7.4	1114; 9.3
	TD	Yes	459; −19.5	299; −7.6	3198; 1.0	2765; 1.2	4794; 0.66	650; 3.1	1060; 13.5	1106; 8.51
	NM	Yes	543; −4.8	–	2063; −34.8	–	–	616; −2.2	890; −4.7	973; −4.6
c	ME1	Yes	494; −13.4	277; −14.4	3110; −1.72	2682; −1.8	4633; −2.7	690; 9.4	856; −8.4	956; −6.2
	EMC	No	418; −26.7	259; −19.8	2996; −5.3	2570; −5.9	4494; −5.6	780; 23.8	692; −25.8	835; −18.1
	ME2	No	399; −30.1	249; −23.1	2950; −6.8	2525; −7.6	4432; −6.9	720; 14.2	638; −31.7	778; −23.7
	P	No	390; −31.6	236; −27.0	2928; −7.5	2504; −8.3	4392; −7.8	695; 10.2	610; −34.7	752; −26.2
d	VP	Yes	565; −1.0	322; −0.4	3213; 1.5	2744; 0.4	4784; 0.4	631; 0.0	934; 0.0	1019; 0.0

3.1.2. Heat transfer between the condensed phase and the volatile products of polymer decomposition/combustion and moisture evaporation

Results obtained using the models with the assumptions listed in point b) are summarized by Fig. 9 (temperature versus time profiles as simulated (lines) and measured ([32], symbols)) at $x = L_{S1}/2$, and Fig. 10 (temperature versus time profiles as simulated (lines) and measured ([12], symbols)) at $x = L_{S1} + L_C + L_{S2}$ for the single skin and the sandwich panels, respectively, and Tables 3 and 4. These models do not produce qualitative changes in the predictions of the process dynamics. As a consequence of the very small moisture contents, quantitative changes induced by the complete absence of moisture (as an "ideal case") are also negligible for the single skin and the sandwich, except for t_{750} in the latter case where it reduces by about 35%. Neglecting the combustion reaction causes an increase in the characteristic times by about 1–10%. Simulations carried out with different fractions of convective heat and mass transport confirm the convective cooling [31] of the hot volatile products leaving the structure. The characteristic times are reduced by about 2–16% ($\alpha = 0$, NHCG) with respect to the case of $\alpha = 1$ assumed by the reference model. The variations induced by the use of one-step thermal decomposition kinetics (instead of oxidative decomposition kinetics) are also small (the maximum is a reduction on t_{625} of 20%). On the whole, as shown by the data listed in Tables 3 and 4, the effects of the combustion of a small fraction of the polymeric resin of the upper skin, thermal (instead of oxidative) decomposition, local thermal equilibrium (and the associated convective cooling) are not items of central importance in the modelling of the systems under study. Instead, moisture evaporation induces large modifications in the temperature profiles along the core thickness with variations on the characteristic times up to 35%.

3.1.3. Models of the effective thermal conductivity for the skins

The influences of the model for the effective thermal conductivity of the skin on the predicted process characteristics are summarized in Fig. 11 which shows the spatial temperature profiles for several times as simulated for the reference case with the S model (dashed lines) and the P model (solid lines) and Fig. 12 (temperature versus time profiles at $x = L_{S1}/2$ as simulated by the five models of effective thermal conductivity and measured [32] for the single skin panel). The simulated values of the selected model outputs are again listed in Table 3. Although not shown (see equations (42)–(44), 47, (58)–(61)), it can be easily verified that the actual values of the effective thermal conductivity increase in the order S, ME1, EMC, ME2 and P model for both the skin and the residue left at the conclusion of the conversion process. For instance, at ambient temperatures the values of the thermal conductivities are, in the order, 0.36, 0.47, 0.52, 0.56 and 0.63 W/mK. Simulation results of the models S, P, ME1, ME2 and EMC show that the effective thermal conductivity model for the skin affects the shape of the temperature profiles and the actual values at the various times and, in this way, the chemical and physical transformations undergone by the panel. The S model is the fastest and presents the best agreement of predicted temperatures with

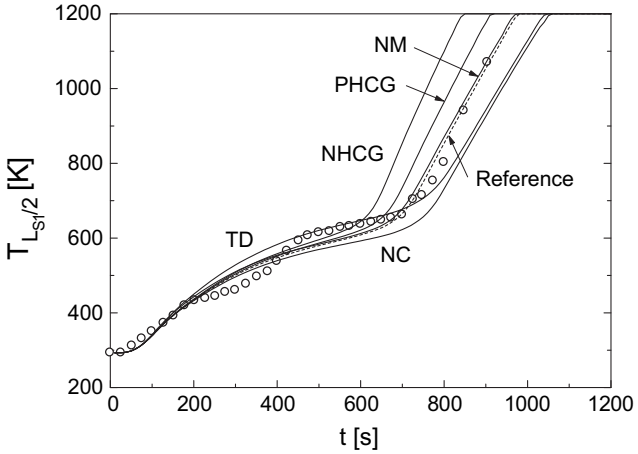

Fig. 9. Predicted (lines) and measured ([32], symbols) temperatures versus time profiles at $x = L_{S1}/2$ for the single skin panel. Predictions are obtained with the reference model ([1], dashed line) and the assumptions of absence of moisture (NM), one-step thermal decomposition kinetics (TD), absence of the combustion step in the polymer conversion mechanism (NC), and no ($\alpha = 0$, NHCG) or partial ($\alpha = 0.5$, PHCG) heat exchange between the condensed phase and the gas phase.

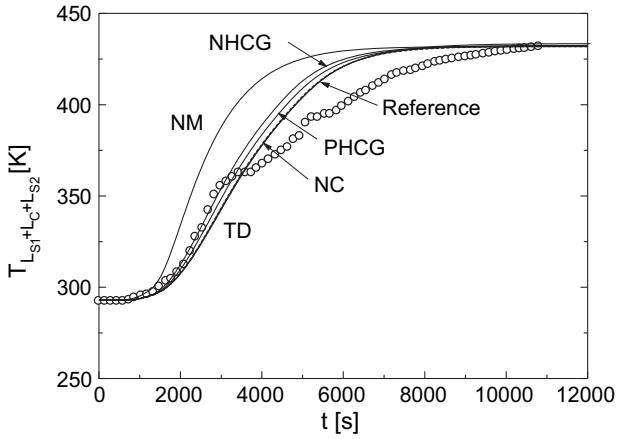

Fig. 10. Predicted (lines) and measured ([12], symbols) temperatures versus time profiles at $x = L_{S1} + L_C + L_{S2}$ for the sandwich panel. Predictions are obtained with the reference model ([1], dashed line) and models based on the same assumptions as in Fig. 9.

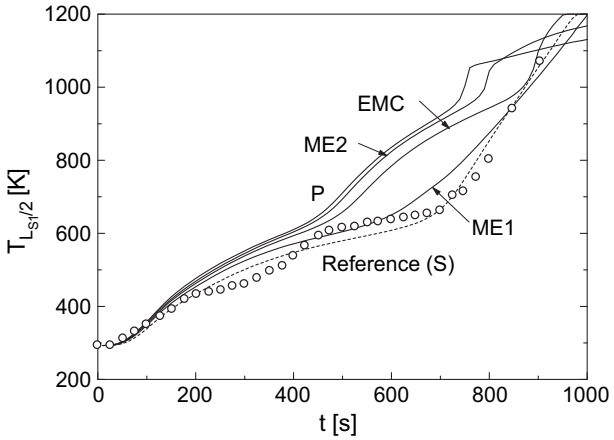

Fig. 12. Predicted (lines) and measured ([32], symbols) temperatures versus time profiles at $x = L_{S1}/2$ for the single skin panel. Predictions are obtained with the reference model ([1], dashed lines) and models with the effective thermal conductivity based on the Parallel (P), the first and second version of the Maxwell–Eucken (ME1, ME2) and Effective Medium Theory (EMT) treatment.

experimental measurements [32]. Indeed, it was preliminarily validated [1] using data [18] for the composite material of interest. Therefore, the comparison with the other models is useful essentially for a sensitivity analysis. Results of the P model show that the heat-exposed surface is constantly at lower temperatures (Fig. 11, differences up to about 350 K). This permits a faster progression of the evaporation and decomposition zones as a consequence of the more rapid heat conduction towards the more internal cold regions. However, the ablation of the heat-exposed surface is delayed and actually begins when the conversion is near to completion. In general, the spatial gradients are significantly lower when compared with the S model (reference case) and the differences become successively larger with the progress of the conversion level. The models of effective thermal conductivity (ME1, ME2, EMC) present intermediate behaviours between those of the S and P models, in accordance with the actual values of the property modelled. In terms of global parameters (Table 3), it can be seen that the influences of the effective thermal conductivity model are quite important. Indeed, the conversion times become shorter by about 7–34% with respect to the reference model. In general, all the characteristic times are shortened but complete ablation never occurs and a residue is left (33–11% of the initial skin length).

The spatial profiles of temperature along the sandwich thickness for several times, as simulated for the P (reference) and S models, are reported in Fig. 13 whereas the temperature versus time profiles at the cold side, as simulated by the various models and measured [12], are plotted in Fig. 14. The effects on the process features are qualitatively similar to those discussed for the single skin panel. As expected, given that the heating dynamics of the sandwich are highly affected by the chemical and physical changes undergone by the heat-exposed skin, the effects of the effective thermal conductivity model of this layer are very strong (for instance, see the times of 400 and 900 s in Fig. 13) until complete ablation is reached. Then, the differences between the temperature profiles tend to disappear (Fig. 13), with a solution that becomes practically independent of the upper skin transients for times longer than about 1800 s. Owing to the significant thermal resistance exerted by the core, the steady temperature profiles established along the lower skin are at too low values for any chemical reaction to occur and, under these conditions, the effects associated with the variations in the model of effective thermal conductivity are small. Therefore, contrary to the case of the single skin panel,

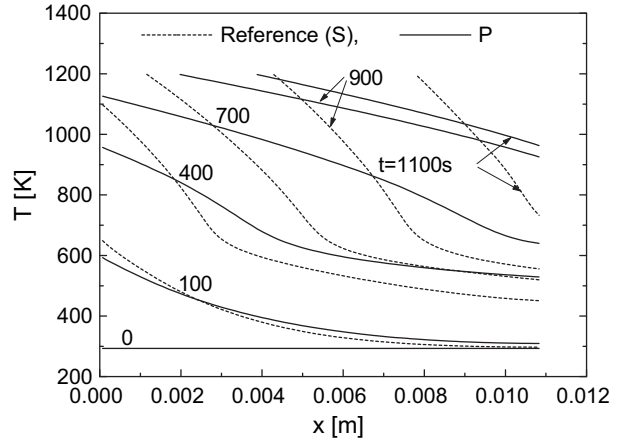

Fig. 11. Temperature profiles along the single skin panel for several times as predicted with the reference model [1] with the Series (S) model for the effective thermal conductivity (dashed lines) and with the Parallel (P) model for the effective thermal conductivity (solid lines).

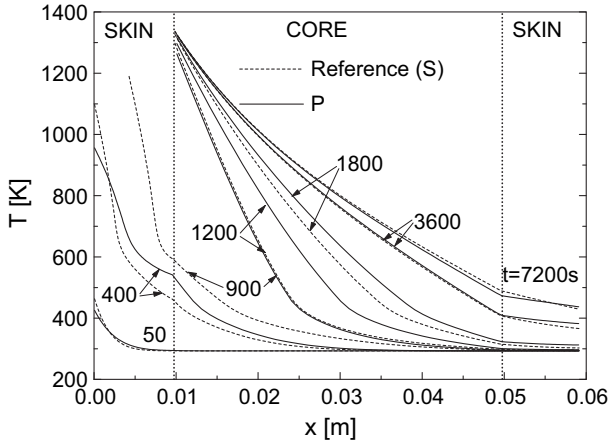

Fig. 13. Temperature profiles along the sandwich panel for several times as predicted with the reference model [1] with the Series (S) model for the effective thermal conductivity (dashed lines) and the Parallel (P) model for the effective thermal conductivity (solid lines).

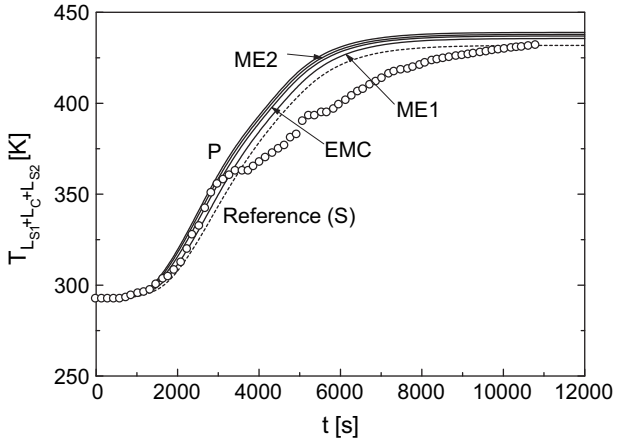

Fig. 14. Predicted (lines) and measured ([12], symbols) temperatures versus time profiles at $x = L_{S1} + L_C + L_{S2}$ for the sandwich panel. Predictions are obtained with the same models as in Fig. 12.

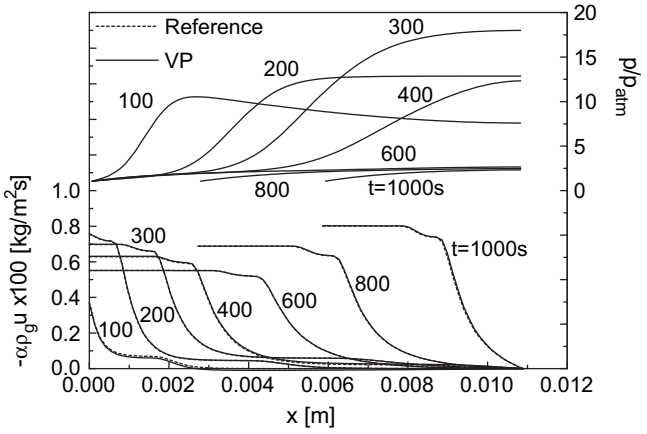

Fig. 15. Pressure and gas mass flux profiles along the single skin panel for several times as predicted with the Variable pressure (VP) model (solid lines). Dashed lines for the gas mass flux are obtained with the reference model [1].

the temporal profiles at the cold side are scarcely dependent on the model of the skin effective thermal conductivity.

In all cases, for the bottom surface of the lower skin (Fig. 14), the predictions slightly anticipate the measured values for times between 3000 and 4000 s owing to the absence of the plateau in the temperature profile at about 373 K reported by the experiments and caused by moisture evaporation. The Arrhenius kinetics for the moisture evaporation rate employed here is slower and describes the release of water vapour over a range of temperature, so that the measured plateau at 373 K is not predicted. From the quantitative point of view, from the S model to the P model, again in accordance with the predictions for the single skin panel, the characteristic times become shorter, except for the beginning of surface ablation. The variation on the parameter t_{750} is relatively small (2–7.5%). Finally, owing to the enhanced heat transfer across the sandwich panel, the H120 test is not verified for the P, ME2 and EMC models.

In general the effective thermal conductivity of composite materials is highly dependent on composition and structure but there is not any single model that is applicable to all types of structures [29] and the five models discussed above are only schematizations of relatively simple situations. Consequently, the comparison of the simulations of the various models can be used to quantify the possible errors made in the selection of one possible schematization instead of another. Finally, it should be noted that the effective thermal conductivity always includes an additional radiative term (eqn. (48)). It results [15] from the assumption that the solid is a matrix with pores of diameter d where heat is exchanged by radiation leading, after linearization, to a contribution proportional to T^3.

3.1.4. Variable pressure model

Results of the simulations carried out with the variable pressure model indicate that, for the single skin panel, the pressure variations are significant (Fig. 15) with maxima up to about 18 atm, but no variation is caused on the mass flux profiles (Fig. 15) and the other relevant process variables. The pressure profile shows a maximum that moves from the heat-exposed surface towards the bottom of the sample where, owing to the assumption of impermeable bottom surface, an almost uniform spatial distribution is established. Large over-pressures (up to a factor of 18) are observed at very short times (about 300 s) and are caused by the release of steam, from moisture evaporation, which accumulates in a medium with a low porosity and permeability. The initial propagation of a high pressure front and the subsequent attainment of high pressures over a large part of the integration domain can be observed (Fig. 15) only before significant decomposition occurs. Then, for times of about 550–600 s, pressures return to nearly the atmospheric value. Indeed, the modified properties of the reacting medium (that is, porosity, permeability, viscosity) permit the rapid flow of the large quantities of volatile products that are generated. Thus the gas velocity is directed towards the heat-exposed surface and is essentially the result of the large amount of volatiles generated. Apart from the initial process transients associated with the evaporation of the small moisture content, the resistance to mass flow is negligible (no differences between the velocity profiles computed for variable or constant gas pressure).

Negligible effects are also caused by the pressure variations across the sandwich panel on the volatile mass flux (Fig. 16) and other process variables. However, the pressure peaks are noticeably lower (maximum values around 10 atm) as a consequence of the large permeability of the core structure and higher total pore volume of the entire structure. The pressure is uniform along the core and, as soon as moisture evaporation across the upper skin is completed, it rapidly decreases. Finally, at very long times, a temporary rise in the pressure is observed, following moisture evaporation, across the lower skin (maximum values around 9 atm at about 4300 s).

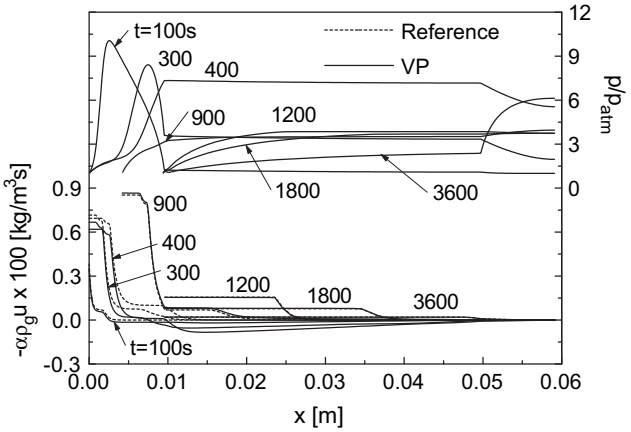

Fig. 16. Pressure and gas mass flux profiles along the sandwich panel for several times as predicted with the Variable pressure (VP) model (solid lines). Dashed lines for the gas mass flux are obtained with the reference model [1].

The negligible influences of pressure variations on the thermal behaviour of degrading solid materials are in qualitative agreement with previous results [2,8,31]. It can be understood that they are important in relation to the structural behaviour of the system and therefore they should be properly taken into account by thermo-mechanical models.

3.2. Sensitivity to model parameters

A sensitivity analysis has been made of the sandwich model for the main input variables (specific heat, thermal conductivity, density and volumetric fraction of the polymeric resin, the glass fibres and the core, parameters for the kinetics of moisture evaporation and polymer decomposition/combustion), with variations comprised between ±25% of the reference values (Table 2). A sensitivity parameter is introduced on several output variables, taken coincident with the characteristic times already introduced, as:

$$\mathrm{SP} = \frac{\dfrac{\varphi_o^{\pm 25\%} - \varphi_o}{\varphi_o}}{\pm 0.25} \tag{69}$$

where φ_o or $\varphi_o^{\pm 25\%}$ is the generic output variable evaluated in correspondence of the generic reference or modified (±25%) input variable. SP = 1 corresponds to a relative variation on the output variable equal to the relative variation on the input variable (with respect to the corresponding reference values). The sensitivity analysis is carried out only for the sandwich model and values of the SP parameter are summarized in Table 5. A high, medium or low sensitivity is assumed when, for at least one of the output variables and a positive or negative change in the input variable, $\mathrm{SP} \gg 1$, $1 > \mathrm{SP} \geq 0.50$, or $0.5 > \mathrm{SP} \geq 0.1$, respectively. A negligible sensitivity is assumed for $\mathrm{SP} < 0.10$.

Sensitivity values well below the threshold of 0.10 (<0.02, not listed in Table 2) are found for the pre-exponential factors of the moisture evaporation rate, the pre-exponential factors of the decomposition and combustion reactions, the order of the combustion reaction, the polymer fraction undergoing combustion and the empirical parameters in the equation for the fibre thermal conductivity (eqn. (47)). High sensitivities are shown only for the activation energies of the moisture evaporation rate, the activation energy of the polymer decomposition rate and the core thermal conductivity. A medium sensitivity is shown by the thermal conductivity, the density and the volume fraction of the polymeric resin, and the core void fraction. The other parameters (see Table 2) show a low sensitivity. Hence the model predictions are not dramatically affected by variations in the input variables that can be considered typical of experimental uncertainty.

As observed from the results already discussed about model assumptions, apart from the expected importance of the external heat flux, it can be seen that the process dynamics are essentially dominated by the external heat transfer rate and, in this way, by the presence of an external heat transfer resistance and/or surface ablation (boundary conditions and related parameter values). These findings are also pertinent to the results obtained from the sensitivity analysis. Indeed, the variations of ±25% on the activation energies, given the Arrhenius law, produce much larger effects on the kinetic rate than the simple linear variation applied to the other input variables (see Table 2), but truly high SP values are observed only for variations in the moisture evaporation rate. This is a low-temperature process and so only partially affected by surface ablation which occurs at much higher temperature. In other words, the variables of the model for the moisture evaporation process present a strong sensitivity because external heat transfer effects are not yet important. On the other hand, the reference values of the other input variables are already capable of exerting their maximum effects and the range of variations examined here is anyway small (i.e. the fibre thermal conductivity).

Table 5
Sensitivity parameter, SP (eqn. (69)), computed by means of the reference model [1] for several characteristic times of the sandwich panel (see definition in Table 4) for variations in several input variables of ±25%. High and medium sensitivities are evidenced.

SP	t_{625}	t_{ds1}	t_{dc}	t_{750}	t_{ds2}	t_{a1}	t_c	t_{a2}
c_{cs+}	0.01	0.04	0.25	0.34	0.20	0.0	0.01	0.02
c_{cs-}	0.01	0.04	0.26	0.34	0.20	0.0	0.01	0.02
c_{f+}	0.13	0.22	0.07	0.05	0.12	0.07	0.12	0.14
c_{f-}	0.14	0.23	0.07	0.05	0.12	0.07	0.12	0.15
c_{p+}	0.14	0.35	0.07	0.05	0.17	0.06	0.09	0.08
c_{p-}	0.14	0.36	0.07	0.05	0.17	0.06	0.09	0.08
d_{c+}	0.0	0.0	−0.04	−0.18	−0.06	0.0	0.0	0.0
d_{c-}	0.0	0.0	−0.05	−0.20	−0.07	0.0	0.0	0.0
d_{s+}	−0.17	−0.01	−0.02	−0.02	−0.01	0.12	−0.07	−0.05
d_{s-}	−0.22	−0.01	−0.02	−0.02	−0.01	0.12	−0.08	−0.05
E_{c+}	0.08	0.02	0.0	0.0	0.0	0.01	0.05	0.0
E_{c-}	0.13	0.10	0.0	0.0	0.0	0.0	0.12	−0.02
E_{d+}	−1.64	−0.57	−0.06	−0.05	−0.04	0.0	0.22	0.17
E_{d-}	−0.27	−3.47	−0.05	−0.07	−2.11	0.0	0.30	0.18
E_{m+}	−0.07	2.95	2.15	0.05	22.24	−0.03	−0.05	−0.04
E_{m-}	−0.11	1.80	1.42	0.48	1.89	−0.06	−0.06	−0.05
k_{cs+}	0.02	0.05	−0.43	−0.57	−0.60	−0.01	0.03	0.03
k_{cs-}	0.03	0.05	−0.64	−1.04	−1.02	0.0	0.04	0.04
k_{p+}	−0.05	−0.39	−0.01	−0.01	−0.05	0.05	−0.06	−0.06
k_{p-}	−0.04	−0.58	0.0	−0.01	−0.08	0.06	−0.06	−0.05
Δh_{d+}	0.38	0.08	0.09	0.08	0.05	0.13	0.30	0.29
Δh_{d-}	0.40	0.09	0.09	0.08	0.05	0.13	0.31	0.30
Δh_{c+}	−0.04	0.0	−0.02	−0.02	−0.01	−0.03	−0.06	−0.08
Δh_{c-}	−0.09	0.01	−0.02	−0.02	−0.01	−0.02	−0.08	−0.08
ε_{cs+}	0.02	0.04	−0.37	−0.40	−0.52	0.01	0.03	0.03
ε_{cs-}	0.02	0.05	−0.48	−0.40	−0.76	0.0	0.03	0.04
ε_{f+}	−0.37	−0.48	−0.08	−0.07	−0.10	−0.17	−0.30	−0.24
ε_{f-}	−0.10	−0.48	−0.05	−0.04	−0.09	−0.26	−0.18	−0.16
ε_{P+}	0.09	0.55	0.05	0.05	0.10	0.33	0.2	0.17
ε_{P-}	0.45	0.55	0.10	0.08	0.12	0.19	0.36	0.29
ρ_{cs+}	0.05	0.12	0.12	0.19	−0.16	0.02	0.07	0.08
ρ_{cs-}	0.05	0.11	0.21	0.41	−0.25	0.01	0.08	0.08
ρ_{f+}	0.14	0.26	0.07	0.06	0.15	0.07	0.13	0.14
ρ_{f-}	0.15	0.26	0.07	0.06	0.15	0.07	0.13	0.15
ρ_{p+}	0.58	0.46	0.18	0.14	0.25	0.25	0.44	0.42
ρ_{p-}	0.60	0.47	0.18	0.14	0.25	0.26	0.46	0.43

4. Conclusions

A model for the thermal response of a glass-fibre/polyester panel and a glass-fibre/polyester–Vermiculux sandwich, previously developed and experimentally validated [1], has been examined for the sensitivity to several model assumptions and the main input parameters. Using the validated model as a reference case (reference model) the following modelling aspects are examined: a) external heating (heating modality in accordance with the assigned boundary conditions and intensity of the heat flux, external heat transfer resistance, surface ablation) and surface heat losses, b) heat transfer between the condensed and the gas/vapour phase, kinetic mechanism and moisture evaporation, c) models for the effective thermal conductivity of the skin panels, d) pressure variations.

Quantitative predictions of the fire behaviour of the structure are highly affected by the simulated imposed heating standards. Variations on the characteristic process times are between 63 and 1379% for the single skin panel and between 49 and 774% for the sandwich panel. Moreover, even for a selected simulated fire exposure, other aspects related to external heating and surface heat losses are predominant. Neglecting the ablation of the external

heated surface (as a model simplification) and the existence of an external heat transfer resistance results in significant modifications in the characteristic times of the process (up to 70%). In the absence of the sole surface ablation, much lower temperatures along both the skin and the core panels are predicted (up to 500–600 K). Heat losses from the non-heated surface are less important for single skin panels (maximum variations between 2 and 9%) than for sandwich structures. In this case, adiabatic lateral surfaces significantly (up to 30%) reduce the heating times for the core. Moreover, a profound alteration in the process dynamics, especially the shape of the temperature profiles and the related values, is observed when no heat losses are permitted from the bottom surface. Indeed, contrary to the reference model, at very long times the lower skin undergoes thermal decomposition and combustion of the polymeric component. The slow heating rates, associated with the presence of a thick chemically inert core, cause the sequential occurrence of the reactions, so that combustion gives rise to temperature peaks up to 1000 K with consequent fire risk problems. Although evaluated for a perfectly adiabatic boundary, this finding emphasizes the importance of adequate thermal exchange for these structures.

Given the small contents, neglecting moisture evaporation does not modify the heating characteristics of the upper skin but its role is important for sandwich panels (modifications in the core heating time up to 35%). The absence of thermal equilibrium between the phases and the disregard of the char combustion step in the reaction mechanism do not introduce significant differences in the predictions (maximum variations on the characteristic process times of 13 and 16% for the single skin and the sandwich panel, respectively), most likely a consequence of the relatively low temperatures typical of polymer decomposition and the small amount of polymeric fraction (char) left for combustion.

The models for the effective thermal conductivity of the fibre-reinforced skin (the Parallel, the Maxwell–Eucken and the Effective Medium Theory models versus the Series model) introduce both qualitative and quantitative differences on the simulated density and temperature profiles along the sandwich panels. Given the experimentally based parameter values, the Series model used in the reference case shows the best performances. The largest differences are observed for the upper skin in the case of the Parallel model with reductions in the characteristic process times up to 35%.

Simulated over-pressures reach high values mainly during the moisture evaporation stage (up to about 10 atm (sandwich)), when the gas porosity and permeability of the structure are still very low. Then, once significant degradation begins, they are rapidly reduced. However, the main features of the thermal response (gas flow, temperature and density profiles) are completely insensitive to pressure variations. Therefore, it can be concluded that pressure variations are important and should be described only when, in addition to the thermal behaviour, the mechanical properties are also modelled.

Finally, the sensitivities of some outputs, taken as representative of the process predictions, to the input variables of the reference model, have been studied. On the whole, it can be stated that the sensitivity to the model inputs is relatively low as the process appears to be dominated mainly by the assumptions made in the formulation of the model, more precisely the conditions of the heat-exposed surface. In detail, it has been found that a strong sensitivity is shown only by the activation energy of the moisture evaporation rate (on the drying times of the two skins and the core with values of the sensitivity parameter in the range 1.4–22), the activation energy of the decomposition reaction (again on the drying times of the two skins and the characteristic heating time of the upper skin with maximum values of the sensitivity parameter in the range delimited by −1.6 and −3.5) and the thermal conductivity of the core (on the heating and drying time with values of the sensitivity parameter up to −1). Lower sensitivities are observed for the polymer thermal conductivity, volumetric fraction and density and the core void fraction.

Acknowledgments

This work is part of the activities carried out in the framework of the project PIROS “Progettazione integrata di componenti multifunzionali per applicazioni in sistemi del settore ferrotranviario e dei vettori di medie dimensioni, associata alla realizzazione di speciali facilities per prove e qualificazioni di materiali in condizioni di fiamma”, coordinated by IMAST and funded by the Italian Ministry of Instruction, University and Research (MIUR), the partial support of which is gratefully acknowledged.

Appendix. Nomenclature

A	Pre-exponential factor [s^{-1}]
c	Specific heat [J/kg K]
d	Pore diameter [m]
E	Activation energy [kJ/mol]
H	Width of the square section of the sample [m]
h_1	Global heat transfer coefficient at the hot face [W/m^2 K]
h_2	Global heat transfer coefficient at the cold face [W/m^2 K]
h_L	Global heat transfer coefficient at the lateral surfaces [W/m^2 K]
k	Thermal conductivity [W/mK]
M	Molecular weight [kg/kmol]
n	Reaction order
p	Pressure [Pa]
Pr	Prandtl number
R	Universal gas constant [kJ/mol K]
Ra	Rayleigh number
S	Specific surface [m^{-1}]
T	Temperature [K]
T_e	Temperature of the external environment [K]
T_f	Flame temperature [K]
t	Time [s]
t_{625}	Time needed to achieve a temperature of 625 K at the centre of either the skin (single skin panel) or the upper skin (sandwich panel) [s]
t_{750}	Time needed to achieve a temperature of 750 K at the centre of the core [s]
t_{a1}	Time corresponding to the beginning of surface ablation [s]
t_{a2}	Time corresponding to the conclusion of surface ablation [s]
t_c	Conversion time for either the skin (single skin panel) or the upper skin (sandwich panel) [s]
t_{dc}	Drying time of the core [s]
t_{ds1}	Drying time of either the skin (single skin panel) or the upper skin (sandwich panel) [s]
t_{ds2}	Drying time of the bottom skin [s]
u	Velocity [m/s]
x	Spatial coordinate [m]
Y	Mass fraction
α	Polimeric mass fraction (kinetic model)
γ	Permeability to gas flow [m^2]
ΔH	Reaction heat [kJ/kg]
ε	Volumetric fraction
λ	Latent heat of water vaporization [kJ/kg]
μ	Gas phase viscosity [Pa s]
ρ	Density [kg/m^3]
σ	Stefan–Boltzman constant [W/m^2K^4]
ψ	Attenuation factor

Subscripts

0	Initial condition
a	Air
ab	Ablation
atm	Atmospheric condition
C	Core
c	Combustion
cr	Critical value
cs	Calcium silicate (Vermiculux)
d	Decomposition
e	Effective
f	Glass fibres
G	Gaseous products of devolatilization and combustion
g	Total gas and vapour
m	Moisture
p	Polymer
r	Residue
S	Skin
v	Steam

Model acronyms

ABS	Adiabatic bottom surface
ABSNC	Adiabatic bottom surface in the absence of the combustion step
ALS	Adiabatic lateral surface
ASTM E119	Standard fire exposure
EMT	Effective Medium Theory model for the effective thermal conductivity
ISO834	Standard fire exposure
ME1	First version of the Maxwell–Eucken model for the effective thermal conductivity
ME2	Second version of the Maxwell–Eucken model for the effective thermal conductivity
NA	Absence of surface ablation
NC	Absence of the combustion step in the polymer conversion mechanism
NHCG	No heat exchange between the condensed phase and the gas phase
NM	Absence of moisture
NPD	Standard fire exposure
NHR	No external heat transfer resistance
NHRNA	No external heat transfer resistance and absence of surface ablation
P	Parallel model for the effective thermal conductivity
PHCG	Partial heat exchange between the condensed phase and the gas phase
S	Series model for the effective thermal conductivity
TD	One-step thermal decomposition kinetics
VP	Variable pressure model

References

[1] Galgano A, Di Blasi C, Branca C, Milella E. Thermal response to fire of a fibre reinforced sandwich panel: model formulation, selection of intrinsic properties and experimental validation. Polym Degrad Stab 2009;94:1267–80.

[2] Di Blasi C. The state of the art of transport models for charring solid degradation. Polym Int 2000;49:1133–46.

[3] Staggs J. Mathematical modelling. In: Horrocks AR, Price D, editors. Fire retardant materials. Cambridge: Woodhead Publishing Limited; 2001. p. 398–420.

[4] Staggs JEJ. Heat and mass transport in developing chars. Polym Degrad Stab 2003;82:297–307.

[5] Davies JM, Wang YC, Wong PMH. Polymer composites in fire. Compos Part A Appl Sci 2006;37:1131–41.

[6] Mouritz AP, Gibson AG. Fire properties of polymer composite materials: Chapter 5: Modelling the thermal response of composites in fire. Dordrecht: Springer; 2006. pp. 133–159.

[7] Di Blasi C, Branca C. A mathematical model for the non-steady decomposition of intumescent coatings. AIChE J 2001;47:2359–70.

[8] Florio J, Henderson JB, Test FL, Hariharan R. A study of the effects of the assumption of local-thermal equilibrium on the overall thermally-induced response of a decomposing, glass-filled polymer composite. Int J Heat Mass Transfer 1991;34:135–47.

[9] http://code.google.com/p/gpyro.

[10] Bozhevolnaya E, Lyckegaard A. Structurally graded core inserts in sandwich panels. Compost Struct 2005;68:23–9.

[11] Mouritz AP, Gardiner CP. Compression properties of fire-damaged polymer sandwich composites. Compos Part A Appl Sci 2002;33:609–20.

[12] Looyeh MRE, Rados K, Bettess P. Thermochemical responses of sandwich panels to fire. Finite Elem Anal Des 2001;37:913–27.

[13] www.marsh.co.uk/Media/Marine-Energy/LCN_Issue2_2007.pdf.

[14] Di Blasi C, Branca C, Sparano S, La Mantia B. Drying characteristics of wood cylinders for conditions pertinent to fixed-bed countercurrent gasification. Biomass Bioenergy 2003;25:45–58.

[15] Gronli MG. A theoretical and experimental study of the thermal degradation of biomass. PhD. thesis, NTNU, Trondheim, Norway; 1996.

[16] www.eaa.net/eaa/education/talat/lectures/2502.pdf.

[17] Drysdale D. An introduction to fire dynamics. New York (NY): John Wiley & Sons, Inc.; 1998.

[18] Perry RH, Green DW, Maloney JO, editors. Perry's chemical engineers' handbook. 6th ed. New York: McGraw-Hill; 1984.

[19] Bai Y, Post NL, Lesko JJ, Keller T. Experimental investigations on temperature–dependent thermo-physical and mechanical properties of pultruded GFRP composites. Thermochim Acta 2008;469:28–35.

[20] Turner IW, Puiggali JR, Jomaa W. A numerical investigation of combined microwave and convective drying of a hygroscopic porous material: a study based on pine wood. Trans IchemE, Part A 1998;76:193–209.

[21] Di Blasi C. Dynamic behaviour of stratified downdraft gasifiers. Chem Eng Sci 2000;21:2931–44.

[22] www.promat.co.uk/fp-products-vermiculux.htm.

[23] Looyeh MRE, Bettess P. A finite element model for the fire performance of GRP panels including variable thermal properties. Finite Elem Anal Des 1998;30:313–24.

[24] Looyeh MRE, Samanta A, Jihan S, McConnachie J. Modelling of reinforced polymer composites subject to thermo-mechanical loading. Int J Num Meth Eng 2005;63:898–925.

[25] Galgano A, Di Blasi C. Modelling wood degradation by the unreacted-core-shrinking approximation. Ind Eng Chem Res 2003;42:2101–11.

[26] Buchanan A. International status of design standards for structural fire safety. In: Proceedings of the NIST-SFPE workshop for development of a national R&D roadmap for structural fire safety design and retrofit of structures. Gaithersburg, MD: NISTIR 7133, National Bureau of Standards. p. 168–83, www.fire.nist.gov/bfrlpubs/fire04/PDF/f04029.pdf; April 2004.

[27] Dodds N, Gibson AG, Dewhurst D, Davies JM. Fire behaviour of composite laminates. Compos Part A Appl Sci 2000;31:689–702.

[28] Carson JK, Lovatt SJ, Tanner DJ, Cleland AC. Thermal conductivity bounds for isotropic, porous materials. Int J Heat Mass Transfer 2005;48:2150–8.

[29] Wang J, Carson JK, North MF, Cleland DJ. A new approach to modelling the effective thermal conductivity of heterogeneous materials. Int J Heat Mass Transfer 2006;49:3075–83.

[30] Bird RB, Stewart WE, Lightfoot EN. Transport phenomena. New York: John Wiley & Sons; 1960.

[31] Di Blasi C. Modelling chemical and physical processes of wood and biomass pyrolysis. Prog Energy Combust 2008;34:47–90.

[32] Krysl P, Ramroth WT, Srewart LK, Asaro RJ. Finite element modelling of fibre reinforced polymer sandwich panels exposed to heat. Int J Num Meth Eng 2004;61:49–68.